ACS OMEGA

http://pubs.acs.org/journal/acsodf

Article

Model for Investigating Relationships between Surfactant Micropollutant Properties and Their Separation from Liquid in a Bubble Column

Arturo A. García-Figueroa,* Boris Albijanic,* Mitzi A. Zarazua-Escobar, Jose L. Lopez-Cervantes, and Jesús Gracia-Fadrique

Cite This: *ACS Omega* 2023, 8, 11717−11724

Read Online

ACCESS | Metrics & More | Article Recommendations | Supporting Information

ABSTRACT: The removal of surfactant micropollutants, such as dyes, pharmaceuticals, and proteins, through foam is very important in biotechnology and wastewater treatment. The literature shows that previous models consider mass balances within the foam but not the adsorption dynamics of micropollutant surfactants on bubble surfaces in the liquid solution. Thus, the main objective of this work is to examine the removal of surfactant micropollutants in a bubble column considering both mass balance and adsorption dynamics to calculate surfactant transport from the liquid bulk to the bubble surface. This allows investigation of the relationships between surfactant hydrophobicity and surfactant separation efficiency from the liquid. It was found that the removal of the surfactant strongly depends on the dynamic adsorption behavior of surfactant on bubble surfaces, and the highest foam fractionation performance was achieved when the surfactant molecule was highly hydrophobic. This work demonstrates that the adsorption dynamics rather than adsorption thermodynamics on bubble surfaces is critical when modeling the removal of surfactant micropollutants from water solutions.

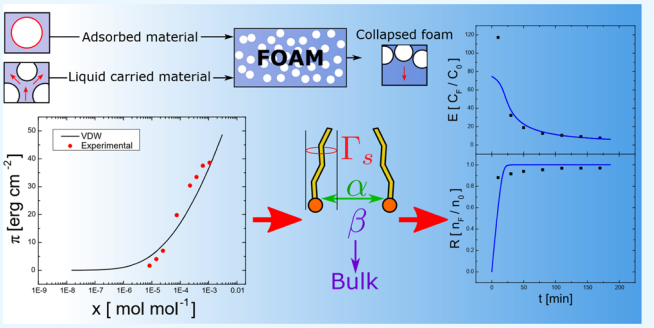

1. INTRODUCTION

During the removal of surfactant micropollutants from a liquid in a bubble column, surfactant molecules are adsorbed on air bubble surfaces, and the generated foam contains a higher amount of the surfactant than the remaining liquid solution.[1] This method is called bubble separation or foam fractionation, which is used in protein purifications,[2−5] pharmaceutical and micropollutant removals,[6−8] and wastewater treatments.[9−11] This is very important considering that some of these chemicals are also surfactants, and foam fractionation is an effective separation method for surfactant removal from a solution containing a low surfactant concentration.

Surfactant properties in liquid solutions and foams are the main driving forces for foam fractionation separations,[12] alongside the hydrodynamics of gas−liquid flow and the mass transfer kinetics. In other words, the chemical structure of surfactants (i.e., cationic, anionic, and non-ionic) may significantly control foam fractionation performances.[13−15] For example, highly hydrophobic molecules are adsorbed strongly on bubble surfaces and removed from the foam phase.[16] Surfactant molecular size also influences surfactant removal since smaller molecules are more concentrated on bubble surfaces.

Different models based on mass balance have been used in the simulation of foam fractionation for different modes of operation and surfactants. For example, Stevenson and Li[17] developed models for continuous operation based on liquid and gas flow through a foam. A mass balance model for the semi-batch foam fractionation operation was developed by Perna et al.,[16] in which a volumetric mass transfer coefficient was used to determine the adsorption of the surfactant on bubble surfaces. Sonc and Grilc[18] and Neely et al.[19] assumed a constant foam−liquid distribution coefficient without explicitly considering the liquid fraction. Maruyama et al.[20] provided the relationship between the surface and bulk concentration of the surfactant in the liquid solution but ignored the dramatic increase in surface tension of the surfactant liquid solution, and the surfactant surface concentration was a fitting parameter obtained from the separation data and the empirical model.

Although the developed models are very useful to simulate foam fractionation processes, all of these models were developed without using surface equations of states and

Received: August 9, 2022
Accepted: February 20, 2023
Published: March 22, 2023

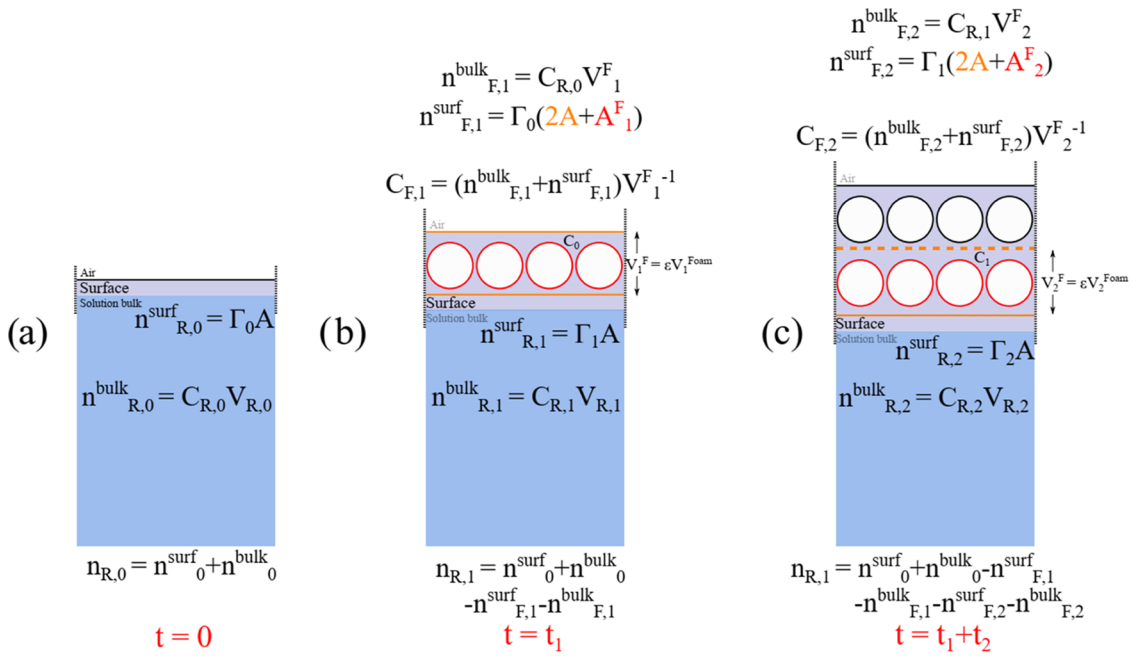

Figure 1. Schematic representation of the foam fractionation model: (a) air−liquid solution surface at $t = 0$; (b) first foam layer formed at $t = t_1$; and (c) second foam layer formed during $t = t_1 + t_2$. Surf was used as an abbreviation for surface.

adsorption isotherms to include surfactant hydrophobicity and surfactant size in the simulations, which allows for predicting surface concentrations of a surfactant. Moreover, all of these models assumed that the surface tension is constant (i.e., the surface tension did not change with operation time), even though in a batch or semi-batch operation, there is a significant increase in surface tension due to the removal of a surfactant. This is very important, considering that the surface tension during foam fractionations can increase by 176% based on our results shown in Section 4.1. Thus, there is a need to use a model which predicts the changes in surfactant surface concentrations using molecular properties, which were quantified using the first principles (i.e., surface equation of state) and not using any empirical relationships. The major objective is to address this matter and to investigate the influence of surfactant properties (i.e., surfactant hydrophobicity and size, as well as interactions between surfactant molecules on bubble surfaces) on foam fractionation performances in a semi-batch operation.

2. MODELING OF SURFACTANT REMOVAL

Changes in surfactant concentration with time in a surfactant liquid solution during foam fractionation in a semi-batch mode were calculated based on a surfactant mass balance and the corresponding surface equations of state and adsorption isotherms. Both equilibrium and dynamic adsorption were considered in this work.

It should be noted that the limitation of the proposed model is that mass transfer kinetics are not considered, such as the film thickness and the interfacial resistance. High surfactant concentrations inducing lyotropic liquid crystal formation are beyond the scope of this model.

Figure 1 shows a schematic representation of the model. At the beginning of the fractionation, i.e., $t = 0$, the bulk and superficial surfactant concentrations are $C_{R,0}$ and Γ_0, respectively (see Figure 1a). Also, at $t = 0$, the cross-sectional area of column A is equal to the area of the air−liquid surface.

The air is introduced into the surfactant liquid solution at time t_1, and a layer of foam is produced. The layer consists of n_b bubbles produced in the sparger of the column, which reaches the air−liquid solution surface ($n_b = 4$ in Figure 1b). For this layer, there are three interfaces: (1) air−foam (of a cross-sectional area of A), (2) air bubble−foam liquid (of an area of A_1^F,*i.e.*, $n_{b1}A_{b1}$ for the n_{b1} bubbles generated with A_{b1} area per bubble), and (3) foam−liquid solution (of a cross-sectional area of A), as seen Figure 1b. Air-foam and air bubble-foam liquid interfaces and foam−liquid solutions have the initial air−liquid solution surface surfactant concentration of Γ_0. The amount of surfactant in the liquid in the first layer in the foam is the sum of the amount of surfactant in this liquid layer in the foam ($C_{R,i-1}V_i^F$), and the amount of surfactant in the interfaces for the first layer $\Gamma_{i-1}(2A + A_i^F)$ and after that, this sum is subtracted from the amount of surfactant drained from the liquid due to the liquid drainage mechanism ($C_{R,i-1}V_i^D$). Stevenson[21] found experimentally that for a foam with a spatially invariant liquid fraction, the liquid drainage velocity is a function of the liquid fraction, the liquid properties in the foam, and the bubble radius (see eq 1).

$$j_{D,i} = \frac{\rho_f g r_b}{\mu_f} m \varepsilon_i^{\,n} \tag{1}$$

where $j_{D,i}$ is the superficial liquid drainage velocity as a function of time; ρ_f and μ_f are the viscosity and density of the liquid in the foam; and m and n are empirical coefficients. In the case of sodium dodecyl sulfate, $m = 0.012$ and $n = 1.74$,[22] and the ρ_f and μ_f in the foam are approximated as these values in the liquid solution. Therefore, the liquid drainage from the foam is expressed as the volume per unit time:

$V_1^D = j_{D,i} A$. The production of these new interfaces depletes surfactant molecules in the liquid solution; therefore, the initial surfactant surface and bulk concentrations of the liquid solution decrease to Γ_1 and $C_{R,1}$, respectively.

At a time of $t = t_1 + t_2$, the second layer of foam is produced, and the system now contains two layers of the foam, see Figure

https://doi.org/10.1021/acsomega.2c05114
ACS Omega 2023, 8, 11717−11724

Table 1. Models for the Surface Equation of State and Their Corresponding Isotherms

name	model (surface equation of state and adsorption isotherm)	assumptions
Langmuir[24]	$\pi = \sigma_{solvent} - \sigma = \Gamma_s R_g T \ln(1 + \beta C)$ $\theta = \frac{\beta C}{1 + \beta C}$	no lateral interactions between adsorbed molecules on a homogeneous surface
van der Waals[25]	$\pi = \sigma_{solvent} - \sigma = \Gamma_s R_g T\left[\frac{\theta}{1-\theta} - \alpha\theta^2\right]$ $\beta C = \frac{\theta}{1-\theta} e^{[(\theta/(1-\theta)) - 2\alpha\theta]}$	long-range weak interactions between adsorbed molecules on a homogeneous surface
Fainerman[26]	$\pi = \sigma_{solvent} - \sigma = -\Gamma_s R_g T\ [\ln(1-\theta) - \alpha_{el}\theta^2]$ $\theta = \frac{\beta C}{1 + \beta C}$	electrically charged double layer on a heterogeneous surface

1c. There is no surfactant flow within layers due to the assumption of negligible liquid drainage from the foam to the liquid solution; a boundary surface between layers is shown in Figure 1c. The second layer of foam has three interfaces: (1) the second foam layer−liquid solution, (2) the air bubble-foam liquid, and (3) the first foam layer-second foam layer. The first foam layer also has three interfaces: (1) air-foam, (2) air bubble-foam liquid, and (3) the first foam layer-second foam layer. The second layer of foam interfaces has a surfactant surface concentration of Γ_1. The production of the second layer depletes surfactant molecules in the liquid solution; therefore, the surfactant surface and bulk concentrations of the liquid solution decrease to Γ_2 and $C_{R,2}$, respectively.

The surfactant concentration is reduced in the liquid solution through foam layer formation. For any foam layer, after the separated foam from the remaining liquid solution is collapsed, the collapsed liquid of the foam, with a volume of V_i^F, has a higher surfactant concentration. The remaining liquid has the volume of $V_{R,i}$. The sum of all of the collapsed foam layers and the remaining liquid volumes represents the initial volume V_0.

The surfactant removed in the collapsed foam at any time is determined by the amount of surfactant carried in the foam liquid $C_{R,i-1}V_i^F$, as well as the adsorbed surfactant at the foam-liquid and the air−liquid interfaces Γ_{i-1} $(2A + A_i^F)$. The removed surfactant concentration in the collapsed foam is given in eq 1.

$$[\text{removed surfactant}]_{t=t} = C_{F,i} = \frac{C_{R,i-1}V_i^F + \Gamma_{i-1}(2A + A_i^F) - V_i^D C_{R,i-1}}{V_i^F - V_i^D} \quad (2)$$

The remaining surfactant concentration is the initial amount of surfactant minus the removed surfactant divided by the remaining liquid volume, as seen in eq 3

$$[\text{remaining surfactant}]_{t=t} = C_{R,i} = \left\{C_0V_0 + \Gamma_0 A - \sum_{i=1}^{t}[C_{i-1}V_i^F + \Gamma_{i-1}(2A + A_i^F) - V_i^D C_{R,i-1}]\right\} \Big/ \left\{V_0 - \sum_{i=1}^{t}(V_i^F - V_i^D)\right\} \quad (3)$$

The volume of the collapsed foam (V_R) and the volume of the foam liquid (V_F) are calculated using eq 4

$$V_F = \varepsilon V_R = \varepsilon\frac{V_g}{1-\varepsilon} = \varepsilon\frac{Q \times t}{1-\varepsilon} \quad (4)$$

where ε is the liquid fraction in the foam, Q is the gas flow rate, and V_g is the gas volume (i.e., $V_g = t \times Q$). The liquid fraction can vary as a function of column height, time, and surfactant concentration.[21] The liquid fraction used was the average liquid fraction of the experimental data.

To calculate the air bubble-foam liquid area (i.e., the sum of all of the bubble surfaces), the bubbles were assumed to be spherical. The total air bubble-foam liquid area is given in eq 5

$$A_i^F = 3V_g r_b^{-1} \quad (5)$$

The bubble radius r_b was used as the average experimental bubble radius.

Wu et al.[23] recovered leaf protein from alfalfa through foam fractionation. Their experimental results showed that the liquid fraction increases at the beginning of the process, and after the first 9 min, the liquid fraction decreases, which was also found in our work (see Section 4.1). Therefore, the liquid fraction can be empirically described using the Gaussian distribution, see eq 6.

$$\varepsilon_i = \varepsilon_0 + \frac{1}{\sigma\sqrt{2\pi}} e^{[-2((t-\mu)/\sigma)^2]} \quad (6)$$

where $\varepsilon_0 = 0.00025$, $\mu = 5$ min, and $\sigma = 0.05$ min.

Table 1 shows a concise review of the most important equilibrium adsorption models used to understand the adsorption of surfactants on gas−liquid interfaces. The Fainerman model was used in all of the simulations, considering that this model was successful in describing surface pressure results in the used concentration interval (see Figure 4). However, other adsorption models were used in Section 4.1.2 to better understand the influence of interactions of surfactant molecules on foam fractionation performance. The Langmuir model and the van der Waals model assume homogeneous surfaces, while the Fainerman model assumes heterogeneous surfaces. It should be noted that for homogeneous surfaces, solvent molecules are not considered in the surface coverage, while the opposite was true for heterogeneous surfaces.

where π is the surface pressure; $\sigma_{solvent}$ is the surface tension of the solvent; σ_i is the surface tension of the surfactant liquid solution at different times; R_g is the universal gas constant, 8.314 J mol^{-1} K^{-1}; T is the temperature; and C is the bulk surfactant fraction. β is the Henry constant. The higher the surfactant surface concentration, the higher the values of β, and β also measures the hydrophobicity of the surfactant molecule.[24] Γ_s is the surfactant surface concentration at the saturation point (i.e., the maximum surface concentration of the surfactant) and is calculated as $1/A_{min}$ (A_{min} represents the minimum area of the surfactant on the liquid surface, leading

https://doi.org/10.1021/acsomega.2c05114
ACS Omega 2023, 8, 11717−11724

to the maximum adsorption of surfactant molecules on the surface). The surface coverage θ is computed as Γ/Γ_s; α is the lateral interactions constant for the van der Waals model. α_{el} is the electrical interaction constant for the Fainerman model.

For the dynamic adsorption, the Ward and Tordai approximation[27] for the short-time adsorption can be used to calculate the surfactant surface concentration and the liquid solution surface tension, see eqs 7 and 8.

$$\Gamma_i = \sqrt{\frac{4D}{\pi}}\, C_{R,i} \tag{7}$$

$$\sigma_i = \sigma_0 - 4RT\sqrt{\frac{D}{\pi}}\, C_{R,i} \tag{8}$$

where D is the surfactant diffusion coefficient in water, i.e., 2.52×10^{-11} m/s^2, σ_i is the surface tension of the surfactant solution at the time i, and σ_0 is the initial surface tension of surfactant solution.

During foam formation, convection may decrease adsorption on bubble surfaces; therefore, we also considered a diffusion-convective adsorption model. Filippov[28] accounted the convective transfer using Levich theory, see eqs 9 and 10.

$$\Gamma_i = \sqrt{\frac{12D}{7\pi}}\, C_{R,i} \tag{9}$$

$$\sigma_i = \sigma_0 - RT\sqrt{\frac{12D}{7\pi}}\, C_{R,i} \tag{10}$$

Finally, the foam fractionation performance is measured with the surfactant enrichment ratio E and recovery R, see eqs 10 and 11

$$E = \frac{C_{F,i}}{C_0} \tag{11}$$

$$R = \frac{V_{F,i}C_{F,i}}{V_0C_0} \tag{12}$$

3. MATERIALS AND METHODS

3.1. Bubble Column. Foam fractionation experiments were conducted using a bubble column, as seen in Figure 2. The air was introduced at a flow rate of 1.42×10^{-5} m^3 s^{-1} through the sparger at the bottom of the bubble column. The bubble column was rectangular, with a cross-sectional area of 1×10^{-3} m^2 and a height of 1 m. The sparger had 6 pores, each with a radius of 1×10^{-3} m.

Sodium dodecyl sulfate surfactant (Merck, 99% purity) was used to compare the calculated and experimental results for surfactant enrichment and recovery. The initial volume and concentration of the surfactant solutions were 2.5×10^{-4} m^3 and 7.54×10^{-4} mol/mol, respectively. The liquid fraction was measured by determining the ratio between the collapsed foam (i.e., liquid) and the noncollapsed foam. Samples of the remaining liquid (<1 mL) were obtained at different times during the process to calculate the surfactant concentration. The liquid surface tension of the samples was measured rapidly after taking the sample using the ring method; the average standard deviation was less than 1%. The removed foam was collected as a function of time, and the surfactant concentration was determined based on the relationship between the surface tension of the liquid and the surfactant concentration.[29−31]

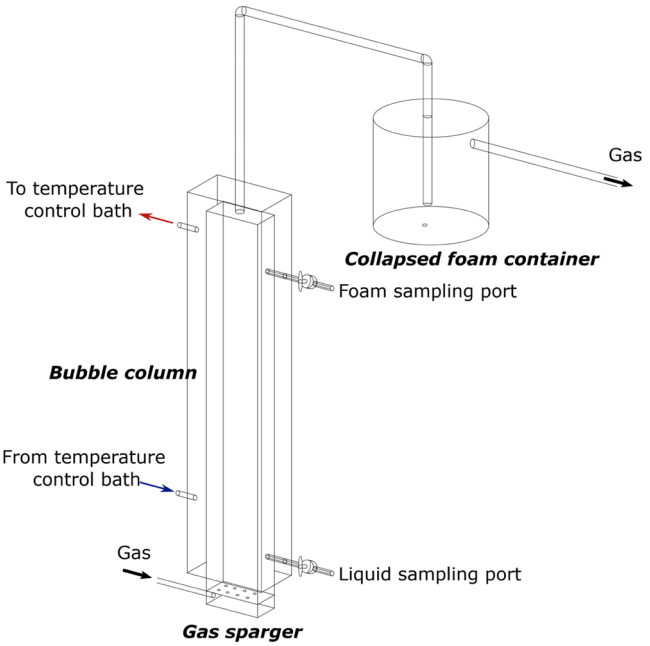

Figure 2. Experimental foam fractionation bubble column.

3.2. Bubble Size. During the foam fractionation process, the changes in bubble size distributions were observed using the imaging technique with a Dino-Lite digital microscope located in front of the column. A 30 Watt white light bulb was used for lighting, and frosted glass was used behind the column to provide a defined background; 10 photographs were taken after 2, 10, 20, and 30 min. All photographs were processed with MATLAB to determine the bubble sizes; the bubble diameter histograms are presented in Figure 3. As seen in Figure 3e, the average bubble size increased from 2 min (0.5 mm) to 10 min (2.2 mm), and after that, it remained constant. It should be noted that bubble coalescence was not significant for surfactant concentrations used in this work, as confirmed using the light dispersion technique (see the Supporting Information).

3.3. Surface Properties of Surfactant Solutions. The Langmuir, van der Waals (VDW), and Fainerman surface equations of state were fitted to the experimental surface pressures, as seen in Figure 4; these models are given in Table 1. It should be noted that the maximum surfactant concentration was below the critical micelle concentration (1×10^{-3} mol/mol). Figure 4 shows that all three models successfully predicted the experimental data.

The obtained fitting parameters are given in Table 2. Further analysis of the foam fractionation using the different surface equations of state and adsorption isotherm is discussed in Section 4.1.1.

4. RESULTS AND DISCUSSION

4.1. Modeling Analysis. The effect of surfactant behavior on bubble surfaces, surfactant hydrophobicity, electrostatic interactions, and surfactant size was analyzed by calculating the remaining surfactant bulk liquid concentration $C_{R,i}$ using eq 3. In these calculations, C_0 is 7.54×10^{-4} mol/mol, V_0 is 2.5×10^{-4} m^3, Q is 6.7×10^{-6} m^3 s^{-1}, the sparger has 6 pores of radius 1×10^{-3} m, and A is 1×10^{-3} m^2.

https://doi.org/10.1021/acsomega.2c05114
ACS Omega 2023, 8, 11717−11724

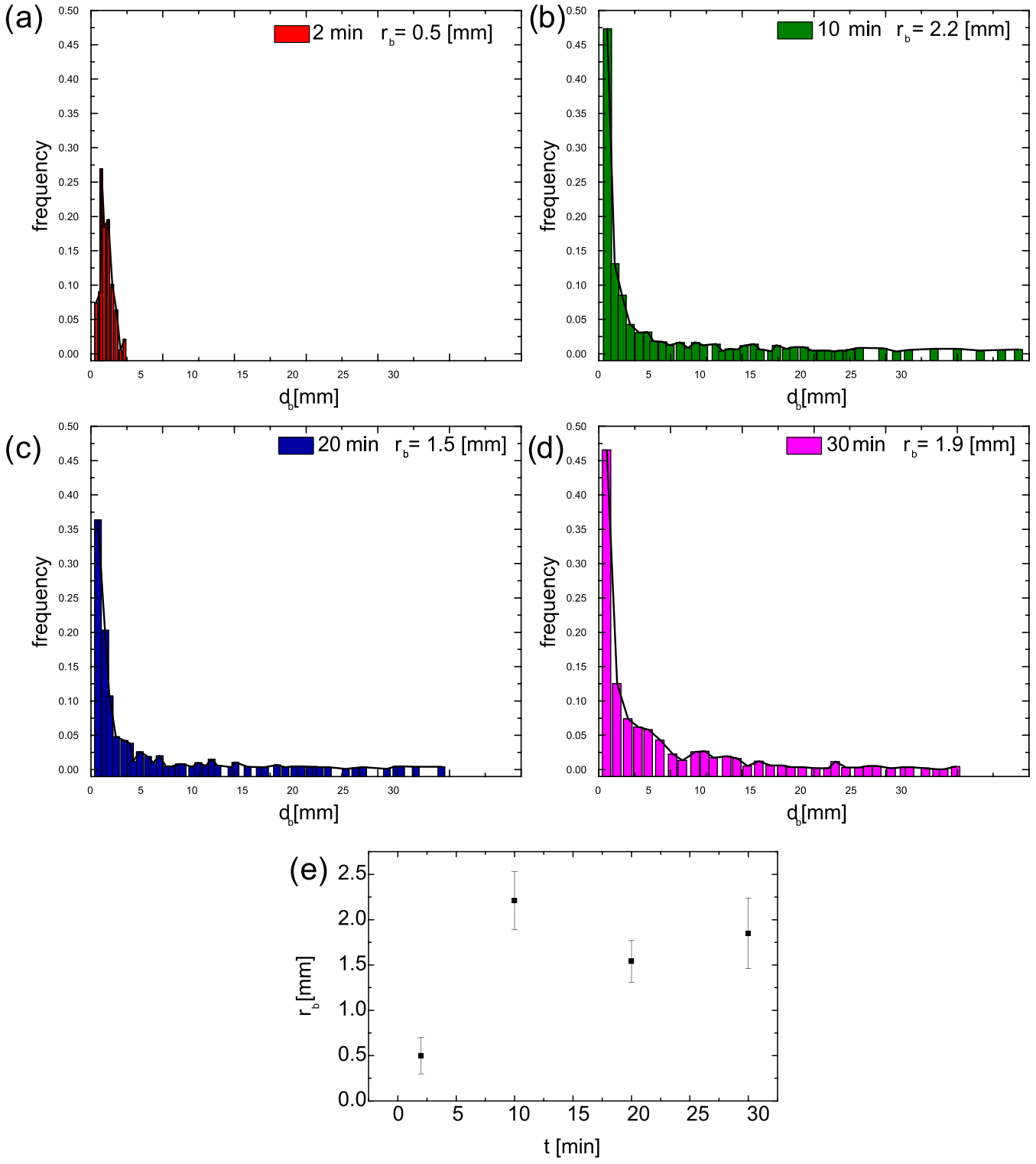

Figure 3. Bubble size distribution during different times of the foam fractionation process of sodium dodecyl sulfate: (a) 2 min, (b) 10 min, (c) 20 min, and (d) 30 min. (e) Average bubble size as a function of process time.

4.1.1. Surfactant Behavior on Bubble Surfaces and Liquid. The Langmuir model does not consider interactions between surfactant molecules on bubble surfaces, while other models consider these interactions (see Table 1). Figure 5a shows that the surface coverage of surfactant molecules on bubble surfaces increased with the molar fraction of surfactant in the solution (i.e., x). The Langmuir model shows the highest surface coverage probably because this model does not consider interactions between surfactant molecules on bubble surfaces. The lowest surface coverage was predicted using the van der Waals model, possibly due to the weak interactions between surfactant molecules on bubble surfaces. When the interactions between surfactant molecules become stronger, as in the Fainerman model, the surface coverage increases. Figure 5b shows that all of the models showed similar predictions of

https://doi.org/10.1021/acsomega.2c05114
ACS Omega 2023, 8, 11717−11724

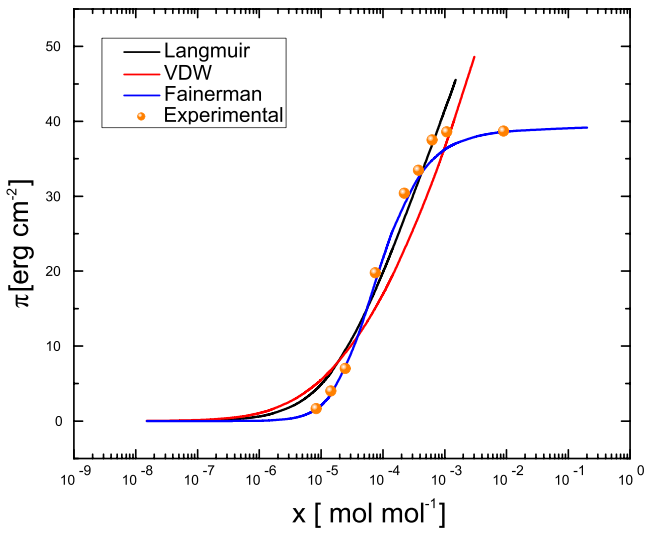

Figure 4. Surface pressure as a function of mass fraction of sodium dodecyl sulfate aqueous solutions.

Table 2. Surface Equation of State Fitting Parameters

model	β	$\Gamma_s R_g T$ [J m^{-2}]	α
van der Waals	63258	0.020	−3
Fainerman	30000	0.020	390
Langmuir	63258	0.009	not applicable

surface pressures. However, the Fainerman model is the only model that shows the surface saturation on bubble surfaces.

The dynamic model best predicts the enrichment and recovery of surfactant, indicating that adsorption of surfactant molecules on bubble surfaces is dynamic adsorption. Although the dynamic model is the most accurate, this model cannot be used to investigate the influence of surfactant hydrophobicity on the foam fractionation process. Thus, in the next section, the Fainerman model was used as an approximation, considering that this model also predicts well the experimental data.

Figure 5c shows that the enrichment of a surfactant decreases near zero for 5 min and then increases near 10 min. This behavior may be explained, because at the beginning of the operation, more liquid than bubbles were transported to the foam phase via liquid, reducing the concentration of a surfactant in a foam phase and thus decreasing enrichment. After 10 min, the amount of surfactant molecules adsorbed on bubble surfaces increases, leading to a higher enrichment. The same trend is observed in Figure 5d, in which there is a change in the slope after 5 min.

It should be noted that the proposed model is available for fast adsorption kinetics on bubble surfaces. This model could also be applied for slow adsorption of a surfactant on bubble surfaces because the model includes the diffusion coefficient, describing the adsorption rate due to diffusion. However, more

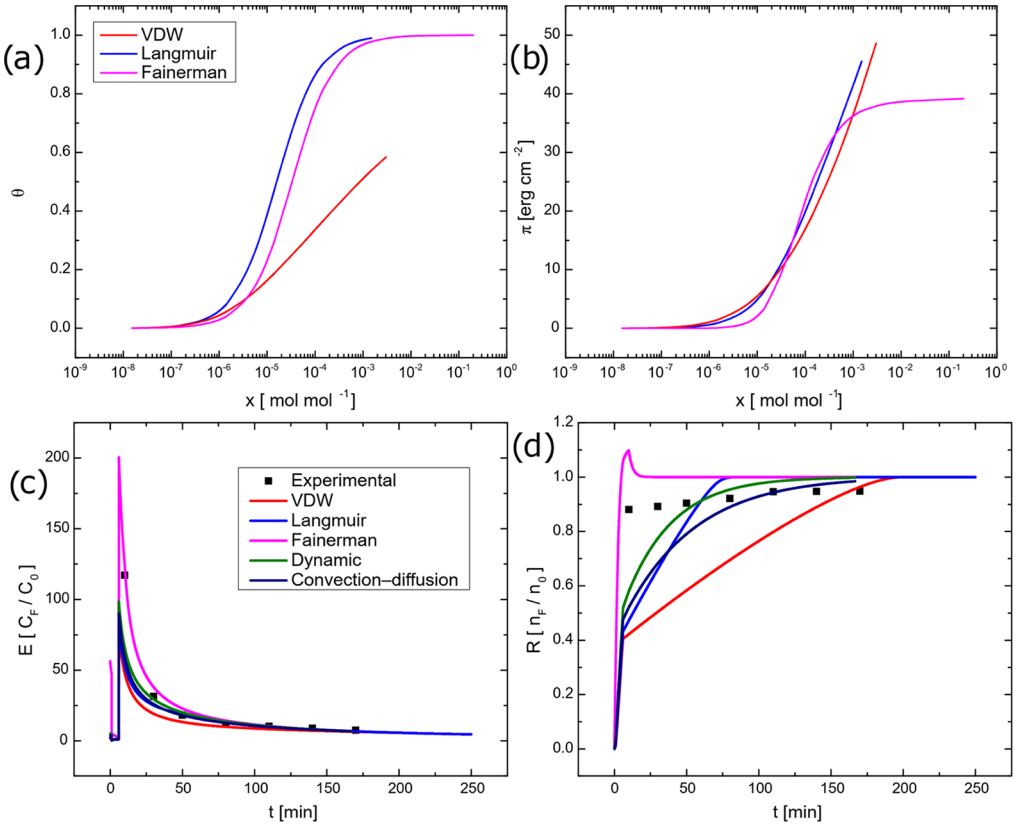

Figure 5. Effect of surfactant behavior on the (a) surface coverage as a function of surfactant mole fraction on aqueous solution, (b) surface pressure as a function of surfactant mole fraction on aqueous solution, foam fractionation (c) enrichment and (d) recovery. The initial concentration was $C_0 = 9.25 \times 10^{-5}$ mol/mol, $V_0 = 2.5 \times 10^{-4}$ m^3, $Q = 1.42 \times 10^{-5}$ m^3 s^{-1}, $\varepsilon = 0.00025$, the sparer has 6 pores of radius 1×10^{-3} m, and A is 1×10^{-3} m^2. For the Langmuir model, the surfactant has $\beta = 63{,}258$ and $\Gamma_s R_g T = 9.96$ mJ m^{-2}; for the van der Waals model, $\beta = 63258$, $\Gamma_s R_g T = 20$ mJ m^{-2}, and $\alpha = -3$; for the Fainerman model, $\Gamma_s R_g T = 20$ mJ m^{-2}, $\beta = 30{,}000$, and $\alpha_{el} = 390$; and for the dynamic and convection−diffusion model, $D = 2.52 \times 10^{-11}$ m s^{-2}.

https://doi.org/10.1021/acsomega.2c05114
ACS Omega 2023, 8, 11717−11724

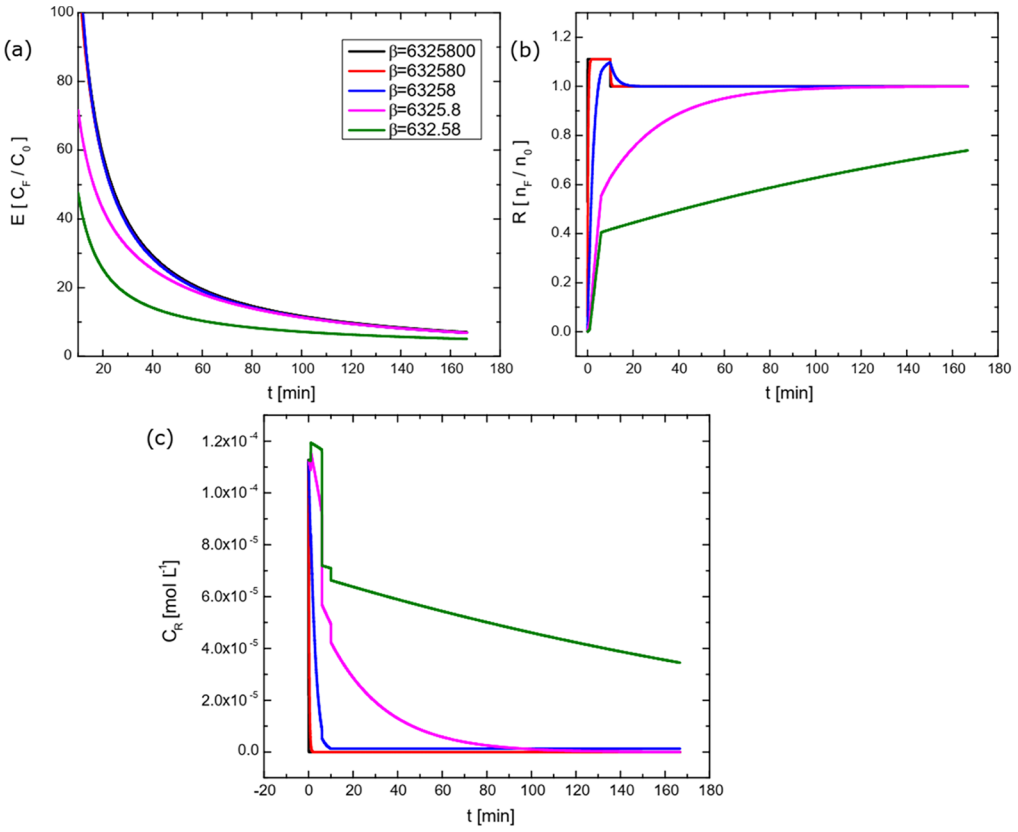

Figure 6. Effect of the surfactant hydrophobicity on the (a) surfactant enrichment ratio, (b) surfactant recovery, (c) remaining surfactant concentration of the liquid solution, and (d) surfactant surface concentration of the liquid solution for a Fainerman-type surfactant with $\Gamma_s R_g T$ = 20 mJ m^{-2}, and a_{el} = 100 with variable surface tension. Q = 6.6 m^3 s^{-1}; ε = 0.00025; 6 pores; A = 10 cm^2; and C_0 = 7.54 × 10^{-4} mol/mol.

experimental data are needed to validate this model for slow adsorption kinetics.

4.1.2. Surfactant Hydrophobicity. Figure 6 shows the influence of surfactant hydrophobicity on the foam fractionation process. The measure of the molecular hydrophobicity is β.[32,33] The higher the surfactant hydrophobicity, the higher the surfactant enrichment ratio (Figure 6a). The reason is that the bubble diameter in the presence of a highly hydrophobic molecule was lower than that in the presence of weakly hydrophobic molecules, which agrees with the results obtained by Jamialahmadi and Müller-Steinhagen.[34] The surfactant enrichment ratio decreased with time, considering that more water and surfactant molecules were transported from the liquid solution to the foam phase as a function of time (see Figure 6a), which leads to a decrease in the remaining surfactant concentration in the liquid solution (see Figure 6c). The surfactant recovery was also the highest for the most hydrophobic surfactant, as seen in Figure 6b, considering that the most hydrophobic surfactant adsorbed more on bubbles, increasing the surfactant recovery. Figure 6c shows a dramatic decrease of the remaining concentration as the hydrophobicity increases because more surfactant molecules are being transported to the surface of bubbles.

5. CONCLUSIONS

This work investigates the influence of surfactant hydrophobicity as well as surfactant adsorption behavior on bubble surfaces on foam fractionation. The proposed model is based on the mass balance for the removal of surfactant from the liquid solution as well as the dynamic adsorption model for short-time adsorption. Although the adsorption of surfactant on bubble surfaces is a dynamic process, the Fainerman model could be used as an approximation, and thus this model is also used in this work. The results showed that the higher the surfactant hydrophobicity, the higher the foam fractionation performance. Further work would be required to investigate anionic, non-ionic, and cationic surfactant properties and their mixture on foam fractionation performances using the proposed model.

■ ASSOCIATED CONTENT

Supporting Information

The Supporting Information is available free of charge at https://pubs.acs.org/doi/10.1021/acsomega.2c05114.

Coalescence inhibition measurements of SDS liquid solutions and coalescence inhibition equipment description (PDF)

■ AUTHOR INFORMATION

Corresponding Authors

Arturo A. García-Figueroa − *Laboratorio de Superficies, Departamento de Fisicoquímica, Facultad de Química, Universidad Nacional Autónoma de México, Ciudad de México 04510, México*; Email: kisuke_urahara92@msn.com

Boris Albijanic − *Western Australian School of Mines: Minerals, Energy, and Chemical Engineering, Curtin University, Kalgoorlie, WA 6430, Australia*; orcid.org/0000-0001-7599-2751; Email: boris.albijanic@curtin.edu.au

https://doi.org/10.1021/acsomega.2c05114
ACS Omega 2023, 8, 11717−11724

Authors

Mitzi A. Zarazua-Escobar − *Laboratorio de Superficies, Departamento de Fisicoquímica, Facultad de Química, Universidad Nacional Autónoma de México, Ciudad de México 04510, México*

Jose L. Lopez-Cervantes − *Laboratorio de Superficies, Departamento de Fisicoquímica, Facultad de Química, Universidad Nacional Autónoma de México, Ciudad de México 04510, México*

Jesús Gracia-Fadrique − *Laboratorio de Superficies, Departamento de Fisicoquímica, Facultad de Química, Universidad Nacional Autónoma de México, Ciudad de México 04510, México;* orcid.org/0000-0002-4681-7986

Complete contact information is available at: https://pubs.acs.org/10.1021/acsomega.2c05114

Notes

The authors declare no competing financial interest.

■ ACKNOWLEDGMENTS

A.A.G.-F. is a doctoral student from Programa de Doctorado en Ciencias Químicas, Universidad Nacional Autónoma de México (UNAM) and received fellowship 739932 from CONACYT, Mexico, under the student number of 411010995. The authors also thank UNAM-DGAPA for the support under the project PAPIIT IG101621.

■ REFERENCES

(1) Pinfold, T. A. Adsorptive Bubble Separation Methods. *J. Sep. Sci.* **1970**, *5*, 379−384.

(2) Lethcoe, K.; Fox, C. A.; Ryan, R. O. Foam fractionation of a recombinant biosurfactant apolipoprotein. *J. Biotechnol.* **2022**, *343*, 25−31.

(3) Koop, J.; Merz, J.; Wilmshöfer, R.; Winter, R.; Schembecker, G. Influence of thermally induced structure changes in diluted β-lactoglobulin solutions on their surface activity and behavior in foam fractionation. *J. Biotechnol.* **2020**, *319*, 61−68.

(4) Wu, Z.; Shu, T.; Zhang, M.; Liu, W. Foam fractionation for effective recovery of leaf protein from alfalfa (*Medicago sativa* L.). *Sep. Sci. Technol.* **2020**, *55*, 1388−1397.

(5) Lockwood, C. E.; Bummer, P. M.; Jay, M. Purification of proteins using foam fractionation. *Pharm. Res.* **1997**, *14*, 1511−1515.

(6) Ghosh, R.; Sahu, A.; Pushpavanam, S. Removal of trace hexavalent chromium from aqueous solutions by ion foam fractionation. *J. Hazard. Mater.* **2019**, *367*, 589−598.

(7) Li, R.; Wu, Z. L.; Wang, Y. J.; Li, L. L. Separation of total saponins from the pericarp of Sapindus mukorossi Gaerten. by foam fractionation. *Ind. Crops Prod.* **2013**, *51*, 163−170.

(8) Su, Y. T.; Han, L.; Ma, H. Y.; Wang, H. S.; Lan, J.; Zhang, Y. Y.; Ying, M. Separation of glycyrrhizic acid by intermittence foam fractionation. *Zhongcaoyao* **2007**, *38*, 365−368.

(9) Tahmouresinejad, H.; Darvishi, P.; Lashanizadegan, A.; Sharififard, H. Treatment of Olefin plant spent caustic by combination of Fenton-like and foam fractionation methods in a bench scale. *Environ. Sci. Pollut. Res.* **2022**, *29*, 1345−1360.

(10) Buckley, T.; Xu, X.; Rudolph, V.; Firouzi, M.; Shukla, P. Review of foam fractionation as a water treatment technology. *Sep. Sci. Technol.* **2022**, *57*, 929−958.

(11) Kumar, A. K.; Ghosh, P. Recovery of an anionic surfactant in the presence of benzene, toluene, and hexane by foam fractionation. *Int. J. Environ. Sci. Technol.* **2022**, *19*, 12345−12356.

(12) Lemlich, R. Adsorptive Bubble Separation Methods—Foam Fractionation and Allied Techniques. *Ind. Eng. Chem.* **1968**, *60*, 16−29.

(13) Srinet, S. S.; Basak, A.; Ghosh, P.; Chatterjee, J. Separation of anionic surfactant in paste form from its aqueous solutions using foam fractionation. *J. Environ. Chem. Eng.* **2017**, *5*, 1586−1598.

(14) Boonyasuwat, S.; Chavadej, S.; Malakul, P.; Scamehorn, J. F. Anionic and cationic surfactant recovery from water using a multistage foam fractionator. *Chem. Eng. J.* **2003**, *93*, 241−252.

(15) Kumar, A. K.; Rawat, N.; Ghosh, P. Removal and recovery of a cationic surfactant from its aqueous solution by foam fractionation. *J. Environ. Chem. Eng.* **2020**, *8*, No. 103555.

(16) Perna, R. F.; Gonçalves, M. C. P.; Santana, C. C. Ascertainment of surfactin concentration in bubbles and foam column operated in semi-batch. *Processes* **2019**, *7*, 154−172.

(17) Stevenson, P.; Li, X. *Foam Fractionation: Principles and Process Design*, 1st ed.; CRC Press: Boca Raton, 2014; p 215.

(18) Sonc, A.; Grilc, V. Batch foam fractionation of surfactants from aqueous solutions. *Acta Chim. Slov.* **2004**, *51*, 687−698.

(19) Neely, C.; Eiamwat, J.; Du, L.; Loha, V.; Prokop, A.; Tanner, R.; Du, J.; Loha, L.; Tanner, A. Modelling a batch foam fractionation process. *Biologia* **2001**, *56*, 583−589.

(20) Maruyama, H.; Seki, H.; Suzuki, A.; Inou, N. Batch foam separation of a soluble protein. *Water Res.* **2007**, *41*, 710−718.

(21) Stevenson, P. Dimensional analysis of foam drainage. *Chem. Eng. Sci.* **2006**, *61*, 4503−4510.

(22) Neethling, S. J.; Lee, H. T.; Cilliers, J. J. A foam drainage equation generalized for all liquid contents. *J. Phys.: Condens. Matter* **2001**, *14*, 331−342.

(23) Wu, Z.; Shu, T.; Zhang, M.; Liu, W. Foam fractionation for effective recovery of leaf protein from alfalfa (*Medicago sativa* L.). *Sep. Sci. Technol.* **2020**, *55*, 1388−1397.

(24) Gracia-Fadrique, J. Langmuir BET Surface Equation of State in Fluid-Fluid Interfaces. *Langmuir* **1999**, *15*, 3279−3282.

(25) Findenegg, G. H. *Soft Matter at Aqueous Interfaces*, 1st ed.; Lang, P.; Liu, Y., Eds.; Springer: Switzerland, 2016; pp 109−136.

(26) Fainerman, V. B.; Lucassen-Reynders, E. H.; Miller, R. Adsorption of surfactants and proteins at fluid interfaces. *Colloids Surf., A* **1998**, *143*, 141−165.

(27) Liu, J.; Xu, Y.; Sun, H. Diffusion-controlled adsorption kinetics of surfactant at air/solution interface. *Chin. J. Chem. Eng.* **2013**, *21*, 953−958.

(28) Filippov, L. K. Dynamic surface tension of aqueous surfactant solutions. *J. Colloid Interface Sci.* **1994**, *164*, 471−482.

(29) Bermúdez-Salguero, C.; Gracia-Fadrique, J. Gibbs Excess and the Calculation of the Absolute Surface Composition of Liquid Binary Mixtures. *J. Phys. Chem. B* **2015**, *119*, 5598−5608.

(30) Li, P. X.; Li, Z. X.; Shen, H. H.; Thomas, R. K.; Penfold, J.; Lu, J. R. Application of the Gibbs Equation to the Adsorption of Nonionic Surfactants and Polymers at the Air−Water Interface: Comparison with Surface Excesses Determined Directly using Neutron Reflectivity. *Langmuir* **2013**, *29*, 9324−9331.

(31) Li, Z. X.; Lu, J. R.; Thomas, R. K.; Rennie, A. R.; Penfold, J. Neutron reflection study of butanol and hexanol adsorbed at the surface of their aqueous solutions. *J. Chem. Soc., Faraday Trans.* **1996**, *92*, 565−572.

(32) Piñeiro, A.; Brocos, P.; Amigo, A.; Gracia-Fadrique, J. The standard Gibbs energy of adsorption from the bulk at the surface of liquid mixtures: reinterpretation of Traube's rule: Analysis of the ΔadsG0 contributions under the Extended Langmuir model. *Fluid Phase Equilib.* **2004**, *225*, 115−123.

(33) Brocos, P.; Gracia-Fadrique, J.; Amigo, A.; Piñeiro, A. Application of the Extended Langmuir model to surface tension data of binary liquid mixtures. *Fluid Phase Equilib.* **2005**, *237*, 140−151.

(34) Jamialahmadi, M.; Müller-Steinhagen, H. Effect of alcohol, organic acid and potassium chloride concentration on bubble size, bubble rise velocity and gas hold-up in bubble columns. *Chem. Eng. J.* **1992**, *50*, 47−56.